Eur J Nucl Med Mol Imaging (2008) 35:630–636
DOI 10.1007/s00259-007-0622-z

ORIGINAL ARTICLE

Biodistribution and radiation dosimetry of the norepinephrine transporter radioligand (*S*,*S*)-[^{18}F]FMeNER-D$_2$: a human whole-body PET study

Akihiro Takano · Christer Halldin · Andrea Varrone · Per Karlsson · Nils Sjöholm · James B. Stubbs · Magnus Schou · Anu J. Airaksinen · Johannes Tauscher · Balázs Gulyás

Received: 5 March 2007 / Accepted: 28 September 2007 / Published online: 14 November 2007

Abstract
Purpose (*S*,*S*)-[^{18}F]FMeNER-D$_2$ is a recently developed positron-emission tomography (PET) radioligand for in vivo quantification of the norepinephrine transporter system. The aim of this study was to provide dosimetry estimates for (*S*,*S*)-[^{18}F]FMeNER-D$_2$ based on human whole-body PET measurements.
Methods PET scans were performed for a total of 6.4 h after the injection of 168.9±31.5 MBq of (*S*,*S*)-[^{18}F]FMeNER-D$_2$ in four healthy male subjects. Volumes of interest were drawn on the coronal images. Estimates of the absorbed dose of radiation were calculated using the OLINDA software.
Results Uptake was largest in lungs, followed by liver, bladder, brain and other organs. Peak values of the percent injected dose (%ID) at a time after radioligand injection were calculated for the lung (21.6%ID at 0.3 h), liver (5.1%ID at 0.3 h), bladder (12.2%ID at 6 h) and brain (2.3%ID at 0.3 h). The largest absorbed dose was found in the urinary bladder wall (0.039 mGy/MBq). The calculated effective dose was 0.017 mSv/MBq.
Conclusion Based on the distribution and dose estimates, the estimated radiation burden of (*S*,*S*)-[^{18}F]FMeNER-D$_2$ is lower than that of [^{18}F]FDG. The radioligand would allow multiple PET examinations in the same research subject per year.

Keywords Dosimetry · Norepinephrine transporter · (*S*,*S*)-[^{18}F]FMeNER-D$_2$

A. Takano · C. Halldin · A. Varrone · P. Karlsson · N. Sjöholm · M. Schou · A. J. Airaksinen · B. Gulyás (✉)
Department of Clinical Neuroscience,
Psychiatry Section, Karolinska Institutet,
Stockholm 171 76, Sweden
e-mail: Balazs.Gulyas@ki.se

J. B. Stubbs
Radiation Dosimetry Systems, Inc,
Palo Alto, CA, USA

J. Tauscher
Lilly Research Laboratories,
Indianapolis, IN, USA

Introduction

The neurotransmitter norepinephrine plays an important role in the regulation of various brain functions, such as affective states, learning and memory, endocrine and autonomic functions. The norepinephrine transporter (NET) is responsible for the reuptake of norepinephrine into the presynaptic nerve terminals [1, 2]. NET plays an important physiological role in the regulation of norepinephrine transmission. Abnormalities in brain NET have been supposed to be associated with a variety of neuropsychiatric diseases such as mood disorder and attention deficit hyperactivity disorder (ADHD) [3, 4]. A NE reuptake inhibitor reboxetine has been observed to be as effective as imipramine and fluoxetine in the treatment of depression [5, 6]. Recently, atomoxetine, a selective norepinephrine reuptake inhibitor (K_i value 5 nM), has been found to be effective for the treatment of ADHD [7–9]. For these reasons, the in vivo imaging of the regional distribution of NET in the human brain has become a research topic of high importance and priority.

The measurement of regional NET levels in the living human brain has been hampered by the lack of suitable positron-emission tomography (PET) radioligands for NET.

^{11}C-labelled *O*-methyl reboxetine analogue, (*S*,*S*)-[^{11}C]MeNER has shown specific binding to NET [10]. However, specific binding to NET did not reach maximal values during the PET scanning session of 93 min (a period stipulated by the 20-min half-time of carbon-11), and the radioligand showed somewhat noisy signal at later time points [10].

Recently, the preparation and evaluation of two novel radiofluorinated analogues of (*S*,*S*)-[^{11}C]MeNER have been reported [11]. PET examination revealed skull-bound radioactivity, contaminating images of the brain and indicating fast defluorination of the radioligand. This defluorination was reduced by the addition of a di-deuterated analogue in PET experiments with (*S*,*S*)-[^{18}F]FMeNER-D$_2$. The use of the latter compound has demonstrated that the in vivo defluorination rate of aryl fluoromethoxy compounds can be reduced through the deuterium isotope effect. (*S,S*)-FMeNER-D$_2$ was found to be almost equipotent to (*S,S*)-MeNER (K_i=3.1 vs 2.5 nM at NET) [11].The di-deutero radioligand (*S,S*)-[^{18}F]FMeNER-D$_2$ was therefore used in the present study. This radioligand has a lower dose exposure to the bone marrow and is supposed to be superior to (*S,S*)-[^{11}C]MeNER given that a specific binding peak equilibrium is reached during the PET experiment at a lower noise level [12].

Radiation dosimetry estimates based on whole-body distribution of activity in monkeys [13] were recently reported for (*S,S*)-[^{18}F]FMeNER-D$_2$. Because of likely species differences [14], the present study was performed with whole-body PET on healthy human subjects to estimate the associated radiation-absorbed doses.

Materials and methods

Radiochemistry

(*S*,*S*)-[^{18}F]FMeNER-D$_2$ was prepared as described in detail elsewhere [11]. The precursor and standard of FMeNER-D$_2$ were supplied by Eli Lilly, Indianapolis, IN, USA. Other chemicals were obtained from commercial sources and were of analytical grade. Radiochemical purity was higher than 99%. The specific radioactivity was higher than 176×10^3 GBq/mmol, and the mass injected was less than 0.4 μg.

Subjects

The study was approved by the Ethics and the Radiation Safety Committees of the Karolinska Hospital. Four male subjects (mean±SD, 25.0±5.9 years) participated after giving informed consent. The study was conducted in line with the Helsinki Declaration and the relevant guidelines of the Karolinska Institute. All subjects were healthy according to medical history, psychiatric interview, physical examination, blood and urine analysis. They did not use any medication 14 days before PET scans, and they were all nonsmokers.

PET data acquisition

Whole-body dosimetry scans were acquired on a Siemens ECAT EXACT 921 PET system, which was run in 2D mode. The transmission scans were acquired using three rotating solid ^{68}Ge rod sources. The ECAT EXACT 921 field of view (FOV) covers 10.8 cm in axial direction and has a patient port of 56.2 cm. The transaxial spatial resolution varies from 6.0 mm full-width at half-maximum (FWHM) in the center of FOV to 6.3 mm FWHM at 10 cm off-center. The PET system was calibrated using a known ^{68}Ge solid cylinder source with a diameter of 20 cm. The calibration interval is dependant on the result of the daily quality control (DQC), which was performed using three rotating solid ^{68}Ge sources. The DQC compares the current status of the detectors with the status at the time of the last normalisation and calibration. Each normalisation was directly followed by a new calibration.

The dosimetry scan protocol was divided into four acquisition stages. The first acquisition stage covered 16 bed positions, approximately 156 cm from head to mid-thigh, while the other acquisition stages covered 12 bed positions, approximately 118 cm. After an intravenous administration of 168.9±31.5 MBq of (*S*,*S*)-[^{18}F]FMeNER-D$_2$, the first acquisition stage was performed using 1-min transmission frames and 2-min emission frames, followed by a 60-min pause. The second acquisition stage was also performed using 1-min transmission frames and 2-min emission frames, although followed by an 80-min pause. The third stage was acquired through 1-min transmission frames and 3-min emission frames, followed by a 40-min pause. The last acquisition stage was performed using 1-min transmission frames and 4-min emission frames. Including scan times, pauses and approximately 17 min for bed movement, the total serial acquisition scan time was 6.4 h.

Data analysis

Brain, heart, liver, kidney, urinary bladder, bone marrow of lumbar vertebra and thyroid were well identified on the first scan images as shown in Fig. 1. Volumes of interest (VOIs) were drawn on the coronal slices of the first scan images with the reference to horizontal and sagittal slices. In the latter three scans, all VOIs except bladder and brain were moved on the same coronal slices to fit the uptake images. VOIs of bladder were drawn flexibly for each scan because the sizes and shapes were changed in scans. VOIs of brain were moved in three dimensions to fit for the latter three scans. An estimate of 9.79% of the active bone marrow in

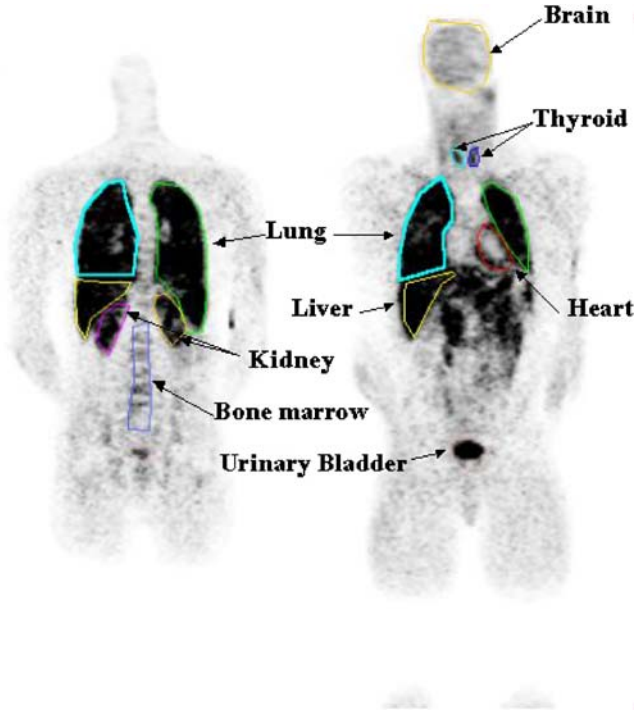

Fig. 1 An example of VOIs for brain, heart, liver, kidney, urinary bladder, bone marrow (lumber vertebra) and thyroid. VOIs were drawn on coronal slices

adults is in the lumbar region of the spine [15]. Thus, the total marrow uptake at any given time was taken as the value from the volume of interest divided by the lumbar fractional distribution value (9.79%).

Radioactivity in VOIs was multiplied by volume of VOIs to get total radioactivity in each source organ.

Residence time calculations

Determining residence times for the source organs requires determining the area under the source organ time–activity curve. Radioactivity in each source organ was expressed as a percentage of the injected dose (%ID) and plotted against time. The time–activity curves, describing the percentage of the injected activity in each source organ as a function of time post-injection, were mathematically simulated. Mono-exponential functions (Eq. 1) were iteratively fit to each source organ's decay-corrected time activity curve using a nonlinear least-squares regression algorithm (SAAM II v 1.2 software; Seattle, USA).

$$A(t) = a_1 \times \exp(-\lambda_1 \times t), \quad (1)$$

where a_1 is the fractional uptake, and λ_1 is its associated biological removal rate (per hour). The residence time, τ, is obtained by analytically integrating the curve-fit equation, $A(t)$ from $t=0$ to infinity, after multiplying each term by the physical decay term [i.e. $\exp(-\lambda_1 \times t)$]. The effective removal rate is the sum of the biological removal rate and the physical decay rate for the nuclide.

For the bone marrow, the decay-corrected lumbar retention values increased from first scan to fourth scan. As such, mono-exponential clearance is not an appropriate mathematical model. To obtain the bone marrow residence times, the trapezoid rule for determining the area under a curve was applied to the non-decay-corrected bone marrow data. In addition, it was assumed that the activity in the marrow at 6 h was cleared only by radioactive decay. The urinary voiding was done between second and third scans for all subjects. One subject also went to void urinary bladder between third and fourth scans. Therefore, the urine activity assumed to be produced at the third scan was the total amount seen at second scan plus the urine at third scan. Similarly, for urine production at fourth scan, the total was the second scan value plus fourth scan value. For the one subject, the total amount of urine activity at fourth scan was considered to be the sum of radioactivity at second, third and fourth scans.

Because the length of the images was different between the first images and the last three images, the estimate for total body retention was derived from the urine accumulation estimates. To obtain an estimate of total body retention, the total body time–activity curves was constructed as 100% of the activity minus the urinary excreted activity. This curve was fit to a mono-exponential function, which was integrated to calculate the total body residence time. The urinary bladder contents' residence time was calculated using Cloutier's dynamic bladder model [16, 17] with voiding intervals of 2.4 and 4.0 h. The remainder of the body residence time was calculated as the corrected total body residence time minus all other residence times, except urinary bladder.

Absorbed dose calculations

The OLINDA software was used to estimate the absorbed doses [18]. Radiation doses were computed for each subject using 2.4-h and 4.0-h bladder voiding intervals. The adult male anthropomorphic model was used to calculate radiation doses for reference adult males using each subject's data. The OLINDA software has a complete series of dosimetry phantoms corresponding to different age "reference human" bodies.

Results

Biodistribution

On the whole body emission images of first scan, lungs, liver, brain, kidneys, urinary bladder, heart, lumber vertebra and thyroid were visually identified as organs with

moderate to high activity (Fig. 2). Non-decay-corrected percentages of injected dose to each organ were plotted against time (Fig. 3a and b). The peak values of the percent injected dose to the lungs, liver, brain, kidneys, heart, bone marrow and thyroid were 21.6, 5.1, 2.3, 1.0, 0.6, 0.4 and 0.06% at peak times 0.3 h. After urine voiding correction, decay-corrected percentage of urinary bladder was 12.2% at peak time 6.0 h (Fig. 4).

Radiation-absorbed dose estimates

Table 1 summarises residence times calculated from whole body images of four subjects. The mean residence time of bone marrow was longest (0.162 h), which was followed by that of lung (0.147 h). In radiation-absorbed dose estimates calculated based on the residence time with 2.4-h urine voiding intervals, the radiation dose of the urinary bladder wall was the highest (0.039 mGy/MBq). The mean effective dose was 0.017 mSv/MBq (Table 2). When 4.0-h urine voiding interval was applied, the mean residence time of urinary bladder was changed from 0.057 to 0.085 h. The radiation dose of the urinary bladder wall was changed from 0.039 to 0.052 mGy/MBq (34% increase). The mean effective dose was changed to 0.018 mSv/MBq (4.9% increase).

Discussion

The present study estimated the dosimetry of (*S*,*S*)-[^{18}F]FMeNER-D_2 based on whole-body PET in human subjects. Highest uptake organ was lungs, followed by liver and brain at peak time. The mean effective dose was 0.017 mSv/MBq.

The effective dose estimated from this study was almost half of that estimated with monkey dosimetry study (0.033 mSv/MBq) [13]. There were several differences to consider between two studies.

First of all, species differences should be considered. There could be some differences in the biodistribution between two species. The metabolism of (*S*,*S*)-[^{18}F]FMeNER-D_2 might be different between monkey and human as reported for other radioligands [19, 20]. The route of elimination seemed mainly the renal system in both human (12%ID at 6 h) and monkey (23%ID at 4.2 h).

Secondly, differences in methodology should be taken into consideration. Human PET scans were performed four times with intervals (6.4 h), whilst the monkey studies were done with one continual epoch for approximately 4.5 h. Due to ethical considerations, one continuous 4.5-h or longer human PET scan was avoided. No dynamic scans were obtained in this study because we preferred static emission scans with longer scan times, consequently, of better image quality, at each time point. The limited number of the time points might result in undersampling of the rapid changes expected in the distribution, which might have effects on residence times.

There were differences of the ways to delineate the regions of interest (ROIs). In this study, we delineated ROIs slice by slice, whilst in the previous monkey study, ROIs were delineated on one "compressed" planar image. A single generous-sized ROI was drawn on each organ in the monkey study. The results with the planar images were reported to be comparable to that of tomographic images with [^{11}C]DASB, but with a slight overestimation (i.e. conservative calculation) of organ radiation burden [21]. However, that single generous ROI was drawn which included all activity in the organ and overlying tissue as well and some amount from adjacent regions. Because the lung uptake was high with (*S*,*S*)-[^{18}F]FMeNER-D_2, the apparent uptake might be increased in the

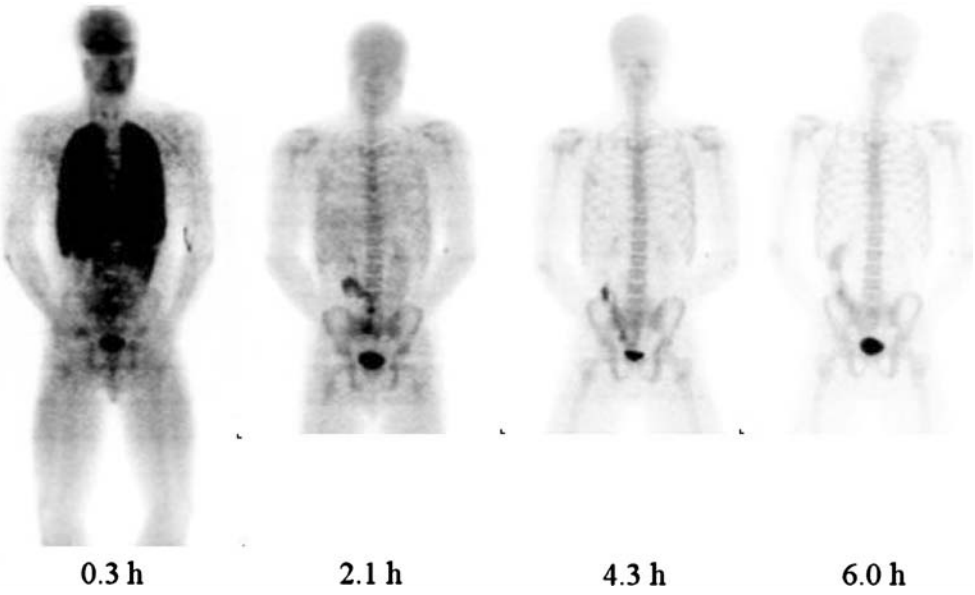

Fig. 2 Typical whole-body images demonstrating biodistribution of (*S*,*S*)-[^{18}F]FMeNER-D_2 in a healthy subject at 0.3, 2.1, 4.3 and 6.0 h after radioligand injection

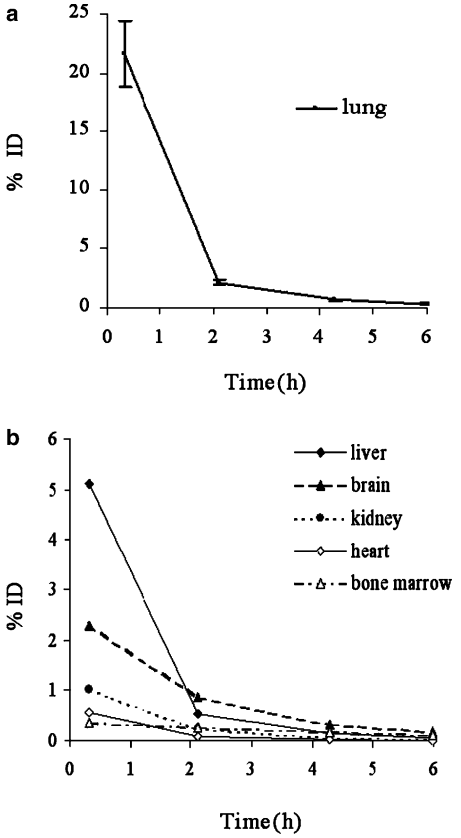

Fig. 3 Mean organ uptake over time without decay correction expressed as a percentage of injected dose (%ID) of (*S*,*S*)-[^{18}F]FMeNER-D$_2$. **a** Lung; **b** liver, brain, kidney, heart, bone marrow and thyroid

surrounding regions such as liver, heart and kidney. The defluorination of (*S*,*S*)-[^{18}F]FMeNER-D$_2$ would show high uptake in the bone in later time. The tissues such as liver, heart and kidney might be overlaid with the spinal column in the planar images, and the apparent uptake might be increased especially in the late phase, resulting in the prolonging of the residence time. The methodological differences of ROI

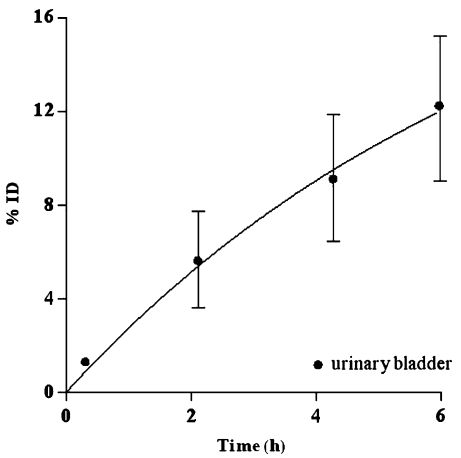

Fig. 4 Mean time activity curve of bladder uptake for (*S*,*S*)-[^{18}F]FMeNER-D$_2$. *Bar* indicates 1 SD. The data were corrected for radioactive decay. The curve overlying the measured data points represents a mono-exponential fitting

Table 1 Residence times calculated from human biodistribution data

Source organ	Residence time (h)
Brain	0.048±0.010
Heart	0.007±0.001
Kidney	0.014±0.004
Liver	0.040±0.011
Lung	0.147±0.023
Bone marrow	0.162±0.018
Thyroid	0.0009±0.0002
Urinary bladder	0.057±0.016
Total body	2.49±0.047
Remainder	2.07±0.056

Values are means±SDs for four subjects.

delineations would show a large difference of the estimated effective doses when applied with ^{18}F radioligands.

The software for the estimation of the effective doses was different between them. The OLINDA software was used to estimate the residence time and radiation doses in this study [18]. The software was created as a replacement for the widely used MIRDOSE3.1 code [22], which was used for the monkey dosimetry study. The OLINDA/EXM 1.0 code is the first computer program to receive approval

Table 2 Radiation dose estimates for (*S*,*S*)-[^{18}F]-FMeNER-D$_2$

Target organ	mGy/MBq	rad/mCi
Urinary bladder wall	0.039±0.007	0.143±0.027
Lungs	0.031±0.004	0.113±0.014
Osteogenic cells	0.023±0.001	0.084±0.002
Red marrow	0.022±0.001	0.080±0.004
Uterus	0.015±0.000	0.054±0.001
Kidneys	0.015±0.002	0.057±0.009
Ovaries	0.014±0.000	0.052±0.000
LLI wall	0.014±0.000	0.050±0.000
Thyroid	0.014±0.002	0.050±0.007
Small intestine	0.013±0.000	0.049±0.001
Pancreas	0.013±0.000	0.049±0.001
Adrenals	0.013±0.000	0.049±0.001
ULI wall	0.013±0.000	0.048±0.001
Gallbladder wall	0.013±0.000	0.047±0.001
Stomach wall	0.012±0.000	0.046±0.001
Spleen	0.012±0.000	0.045±0.001
Total body	0.012±0.000	0.043±0.000
Thymus	0.012±0.000	0.043±0.001
Heart wall	0.012±0.000	0.043±0.002
Muscle	0.011±0.000	0.040±0.001
Testes	0.011±0.000	0.040±0.000
Brain	0.011±0.002	0.039±0.006
Liver	0.010±0.001	0.038±0.005
Breasts	0.009±0.000	0.035±0.001
Skin	0.008±0.000	0.031±0.001
	mSv/MBq	rem/mCi
Effective dose equivalent	0.018±0.001	0.067±0.003
Effective dose	0.017±0.001	0.062±0.002

A 2.4-h urine voiding interval was assumed.

from the FDA to be distributed after 510(k) premarket notification. Agreement of doses between the MIRDOSE3.1 and OLINDA/EXM codes was reported to be good within 1–2% [18]. It does not seem that the difference of the software would explain such difference between the two results from the monkey and human study. The lung uptake of (*S*,*S*)-[^{18}F]FMeNER-D$_2$ was high as reported with other monoamine transporter radioligands such as [^{11}C]McN5652 and [^{11}C]DASB [20, 23]. Although the lung has binding sites for 5-HT transporter [24], (*S*,*S*)-[^{18}F]FMeNER-D$_2$ has quite low affinity to 5-HT transporter [11]. A possible mechanism of the lung accumulation is non-specific uptake of amine by the macrophages in the lungs [24]. Another developed NET radioligand, [^{11}C]MRB, was reported to have lung uptake, but no inhibition of lung uptake by SNRI [25]. This indicates that the lung uptake of (*S*,*S*)-[^{18}F]FMeNER-D$_2$ might be mainly non-specific.

The effective dose estimated in this study was comparable to the other [^{18}F]-labelled radioligands such as [^{18}F]FDG (0.019–0.024 mSv/MBq) [26, 27], [^{18}F]FPCIT (0.012 mSv/MBq) [28], [^{18}F]FECNT (0.0158 mSv/MBq) [29].

Regarding total radioactivity needed to have an acceptable brain image quality for (*S*,*S*)-[^{18}F]FMeNER-D$_2$, we have not investigated at which levels the injected radioactivity can be minimised to. From our previous preliminary human brain study, we might say that more than 100 MBq would be needed to get an acceptable image quality for dynamic data [30].

Guidelines on radiation exposure for human subjects involved in research studies vary widely internationally. The European Commission has established the medical exposures directive (97/43/Euratom), which contains three categories of effective dose ranges applied for adults under 50 year s of age [31]. Under these guidelines, radiation dose is categorised according to the risk-to-benefit level. When the benefit of a research project should probably be related to "increase in knowledge leading to health benefit", corresponding effective dose range is 0.1–1 mSv (Category IIa). When the benefit of a research project would be expected to be "aimed directly at the diagnosis, cure ore prevention of disease", corresponding effective dose range is 1–10 mSv (Category IIb). (*S*,*S*)-[^{18}F]FMeNER-D$_2$ was the only radioligand available for NET. NET was considered to be involved in several psychiatric diseases such as mood disorder and ADHD. NET is a main target for drugs for such diseases. Considering the expected application of this radioligand, Category IIb would be appropriate. Maximal limit of 10 mSv would result from an injected activity of 600 MBq of (*S*,*S*)-[^{18}F]FMeNER-D$_2$ per subject per year.

On the other hand, 5 mSv has been reported as the average radiation dose per patient from nuclear medicine procedures in Europe [32, 33]. Based on this report, approximately 300 MBq of (*S*,*S*)-[^{18}F]FMeNER-D$_2$ could be injected per subject per year.

In the USA, for radiopharmaceutical administration with the approval of a Radioactive Drug Research Committee, the radiation dose to be received by research patients is limited to 30 mSv per dose and 50 mSv per annum to total whole-body, active blood-forming organs, gonads and lens of the eye (10 CFR 21, PART 361). The single-dose limit to other organs is 50 mSv per injected dose and 150 mSv per annum (10 CFR 21, PART 361). Based on the data presented here, the absorbed dose in the urinary bladder wall limits (*S*,*S*)-[^{18}F]FMeNER-D$_2$ radioactivity to be injected in a single dose to 1280 MBq in the adult, with up to three such injections per annum.

There were some limitations in the present study. We performed PET scans only for four male subjects. The number of the subjects was small. However, the deviation of the results from four subjects was not so large. It would be needed in future study for the sex differences of the distribution and dose burden.

Urine collections were not done in this study. They would give us more detailed analysis for radiation burden of the bladder wall. However, healthy subjects were usually able to void the entire amount of activity accounted for in the urine bladder ROIs. Therefore, we think that the addition of the radioactivity in the previous scan to that in the next scan would give us reasonable results for cumulative urine excretion.

For the bone marrow estimates, we took a VOI of the lumbar region and used the percentage of marrow in the lumbar region as published in the Adult anthropomorphic phantom series of Cristy and Eckerman [15]. Although this document did not provide magnitude of potential errors in this number (9.79%), there are also potential differences in the size of the VOI used on each subject. When the bone marrow residence time was simulated to increase by 33%, radiation dose estimates would increase by 17% in bone marrow and by 8% in osteogenic cells, respectively, and effective dose would increase by 2% (data not shown).

In conclusion, the estimated radiation burden of (*S*,*S*)-[^{18}F]FMeNER-D$_2$ was 0.017 mSv/MBq based on the distribution and dose estimates in the human body. Although the practical injection radioactivity might vary among countries, it would allow multiple PET examination on the same research subject per year.

Acknowledgements The authors would like to thank Lilly Research Laboratories for providing the precursors and standards. We are grateful to all members of the PET group at the Karolinska Institutet. We also thank Pierre Lafolie for subject recruitment.

References

1. Blakely RD, De Felice LJ, Hartzell HC. Molecular physiology of norepinephrine and serotonin transporters. J Exp Biol 1994;196:263–81.
2. Galli A, DeFelice LJ, Duke BJ, Moore KR, Blakely RD. Sodium-dependent norepinephrine-induced currents in norepinephrine-

transporter-transfected HEK-293 cells blocked by cocaine and antidepressants. J Exp Biol 1995;198:2197–212.
3. Biederman J, Spencer T. Attention-deficit/hyperactivity disorder (ADHD) as a norepinephrine disorder. Biol Psychiatry 1999;46: 1234–42.
4. Roy A, Pickar D, De Jong J, Karoum F, Linnoila M. Norepinephrine and its metabolites in cerebrospinal fluid, plasma, and urine. Relationship to hypothalamic-pituitary-adrenal axis function in depression. Arch Gen Psychiatry 1988;45:849–57.
5. Berzewski H, Van Moffaert M, Gagiano CA. Efficacy and tolerability of reboxetine compared with imipramine in a double-blind study in patients suffering from major depressive offsodes. Eur Neuropsychopharmacol 1997;7(Suppl 1):S37–47.
6. Massana J. Reboxetine versus fluoxetine: an overview of efficacy and tolerability. J Clin Psychiatry 1998;59(Suppl 14):8–10.
7. Spencer T, Biederman J, Wilens T, Prince J, Hatch M, Jones J, et al. Effectiveness and tolerability of tomoxetine in adults with attention deficit hyperactivity disorder. Am J Psychiatry 1998;155:693–5.
8. Michelson D, Faries D, Wernicke J, Kelsey D, Kendrick K, Sallee FR, et al. Atomoxetine ADHD Study Group. Atomoxetine in the treatment of children and adolescents with attention-deficit/hyperactivity disorder: a randomized, placebo-controlled, dose-response study. Pediatrics 2001;108:E83.
9. Bymaster FP, Katner JS, Nelson DL, Hemrick-Luecke SK, Threlkeld PG, Heiligenstein JH, et al. Atomoxetine increases extracellular levels of norepinephrine and dopamine in prefrontal cortex of rat: a potential mechanism for efficacy in attention deficit/hyperactivity disorder. Neuropsychopharmacology 2002;27:699–711.
10. Schou M, Halldin C, Sovago J, Pike VW, Gulyas B, Mozley PD, et al. Specific in vivo binding to the norepinephrine transporter demonstrated with the PET radioligand, (S,S)-[^{11}C]MeNER. Nucl Med Biol 2003;30:707–14.
11. Schou M, Halldin C, Sovago J, Pike VW, Hall H, Gulyas B, et al. PET evaluation of novel radiofluorinated reboxetine analogs as norepinephrine transporter probes in the monkey brain. Synapse 2004;53:57–67.
12. Seneca N, Gulyas B, Varrone A, Schou M, Airaksinen A, Tauscher J, et al. Atomoxetine occupies the norepinephrine transporter in a dose-dependent fashion: a PET study in nonhuman primate brain using (S,S)-[^{18}F]FMeNER-D$_2$.Psychopharmacology (Berl) 2006;188:119–27.
13. Seneca N, Andree B, Sjoholm N, Schou M, Pauli S, Mozley PD, et al. Whole-body biodistribution, radiation dosimetry estimates for the PET norepinephrine transporter probe (S,S)-[^{18}F]FMeNER-D$_2$ in non-human primates. Nucl Med Commun 2005;26:695–700.
14. Wrobel MC, Carey JE, Sherman PS, Kilbourn MR. Simplifying the dosimetry of carbon-11-labeled radiopharmaceuticals. J Nucl Med 1997;38:654–60.
15. Cristy M, Eckerman KF. Specific absorbed fractions of energy at various ages from internal photon sources. I. Methods. ORNL/TM-8381/V1 (Oak Ridge National Laboratory), April 1987.
16. Cloutier RJ, Smith SA, Watson EE, Snyder WS, Warner GG. Dose to the fetus from radionuclides in the bladder. Health Phys 1973;25:147–61.
17. Stabin MG, Siegel JA. Physical models and dose factors for use in internal dose assessment. Health Phys 2003;85:294–310.
18. Stabin MG, Sparks RB, Crowe E. OLINDA/EXM: the second-generation personal computer software for internal dose assessment in nuclear medicine. J Nucl Med 2005;46:1023–7.
19. Fowler JS, Ding YS, Logan J, MacGregor RR, Shea C, Garza V, et al. Species differences in [^{11}C]clorgyline binding in brain. Nucl Med Biol 2001;28:779–85.
20. Lu JQ, Ichise M, Liow JS, Ghose S, Vines D, Innis RB. Biodistribution and radiation dosimetry of the serotonin transporter ligand ^{11}C-DASB determined from human whole-body PET. J Nucl Med 2004;45:1555–9.
21. Tipre DN, Lu JQ, Fujita M, Ichise M, Vines D, Innis RB. Radiation dosimetry estimates for the PET serotonin transporter probe ^{11}C-DASB determined from whole-body imaging in non-human primates. Nucl Med Commun 2004;25:81–6.
22. Stabin MG. MIRDOSE: personal computer software for internal dose assessment in nuclear medicine. J Nucl Med 1996;37:538–46.
23. Takano A, Suhara T, Sudo Y, Inoue M, Hashimoto K, et al. Comparative evaluation of two serotonin transporter ligands in the human brain: [^{11}C](+)McN5652 and [^{11}C]cyanoimipramine. Eur J Nucl Med Mol Imaging 2002;29:1289–97.
24. Suhara T, Sudo Y, Yoshida K, Okubo Y, Fukuda H, Obata T, et al. Lung as reservoir for antidepressants in pharmacokinetic drug interactions. Lancet 1998;351:332–5.
25. Ding YS, Lin KS, Garza V, Carter P, Alexoff D, Logan J, et al. Evaluation of a new norepinephrine transporter PET ligand in baboons, both in brain and peripheral organs. Synapse 2003;50:345–52.
26. Mejia AA, Nakamura T, Masatoshi I, Hatazawa J, Masaki M, Watanuki S. Estimation of absorbed doses in humans due to intravenous administration of fluorine-18-fluorodeoxyglucose in PET studies. J Nucl Med 1991;32:699–706.
27. International Commission on Radiological Protection. ICRP Publication 80. Radiation dose to patients from radiopharmaceutical. Ann ICRP 1998;p 28.
28. Robeson W, Dhawan V, Belakhlef A, Ma Y, Pillai V, Chaly T, et al. Dosimetry of the dopamine transporter radioligand ^{18}F-FPCIT in human subjects. J Nucl Med 2003;44:961–6.
29. Deterding TA, Votaw JR, Wang CK, Eshima D, Eshima L, Keil R, et al. Biodistribution and radiation dosimetry of the dopamine transporter ligand. J Nucl Med 2001;42:376–81.
30. Takano A, Gulyas B, Varrone A, Karlsson P, Schou M, Airaksinen A, Vandenhende F, Tauscher J, Halldin C. Imaging the norepinephrine transporter with positron emission tomography: initial human studies with (*S,S*)-[^{18}F]FMeNER-D$_2$. Eur J Nucl Med Mol Imaging 2007; 48:247.
31. Guidance on medical exposures in medical and biomedical research. Radiation Protection 99. European Commission 1998.
32. Beekhuis H. Population radiation absorbed dose from nuclear medicine procedures in The Netherlands. Health Phys 1988; 54:287–91.
33. International Commission on Radiological Protection. ICRP Publication 73.Radiological Protection and Safety in Medicine. Ann ICRP 1996;p 26.